Environ Geol (2007) 51: 1133–1145
DOI 10.1007/s00254-006-0404-0

ORIGINAL ARTICLE

Carmine Apollaro
Luigi Marini
Rosanna De Rosa

Use of reaction path modeling to predict the chemistry of stream water and groundwater: a case study from the Fiume Grande valley (Calabria, Italy)

Received: 29 April 2006
Accepted: 12 June 2006
Published online: 11 July 2006

C. Apollaro · R. De Rosa
Department of Earth Sciences,
University of Calabria,
via Ponte Bucci 4, cubo 15B,
87036 Arcavacata di Rende (CS), Italy
E-mail: apollaro@unical.it
E-mail: derosa@unical.it

L. Marini (✉)
Laboratory of Geochemistry, Dip.Te.Ris.,
Genoa University, Corso Europa 26,
16132 Genoa, Italy
E-mail: lmarini@dipteris.unige.it
Tel.: +39-010-3538307
Fax: +39-010-352169

Abstract The irreversible water–rock mass exchanges leading to the production of the Fiume Grande valley (Calabria, Italy) stream waters and groundwaters, starting from local rainwaters, were simulated through reaction path modeling in reaction progress (stoichiometric) mode. The simulations assumed bulk dissolution of a phyllitic rock and calcite and precipitation of gibbsite, kaolinite, amorphous silica, illite, a smectite solid mixture, a hydroxide solid mixture, and a trigonal carbonate solid mixture. The analytical contents of major and trace elements in stream waters and groundwaters were satisfactorily reproduced. However, further investigations are necessary to clarify the fate of As in this natural systems.

Keywords Geochemistry · Groundwater · Stream water · Reaction path modeling

Introduction

In recent years, several efforts of the geochemical community have been devoted to elucidate the fate of trace elements and especially of potentially hazardous elements and species (PHES) in different geological media such as soils, stream sediments, surface waters and groundwaters. Arsenic plays a pivotal role among PHES owing to its very high toxicity and has been the subject of several researches (e.g., Smedley e Kinniburgh 2002 and references therein).

In Italy, existing geochemical data on stream sediments gathered during different mining exploration surveys have been recently re-evaluated during a research project funded by ANPA (the National Environmental Protection Agency) and CNR (the National Research Council) with the aim to assess natural backgrounds, or geochemical baselines (Ottonello and Serva 2003). In the Calabria Region this exercise evidenced the presence of an important As anomaly in the Fiume Grande catchment (Apollaro et al. 2003). This finding prompted the execution of further studies aimed at acquiring detailed information on the composition of soils, stream sediments, groundwaters, and stream waters to confirm such an As anomaly in stream sediments and investigate the possible exchange of chemical elements (especially As and other PHES) among the different geological media (Apollaro 2005).

Here, the EQ3/6 Software Package, version 7.2 (Wolery 1979, 1992; Wolery and Daveler 1992) is used for modeling the irreversible water–rock mass exchanges and provide the theoretical framework for the interpretation of analytical data of natural waters, based on the assumption that the evolution of local rainwaters to stream waters and groundwaters can be satisfactorily simulated through reaction path modeling in reaction

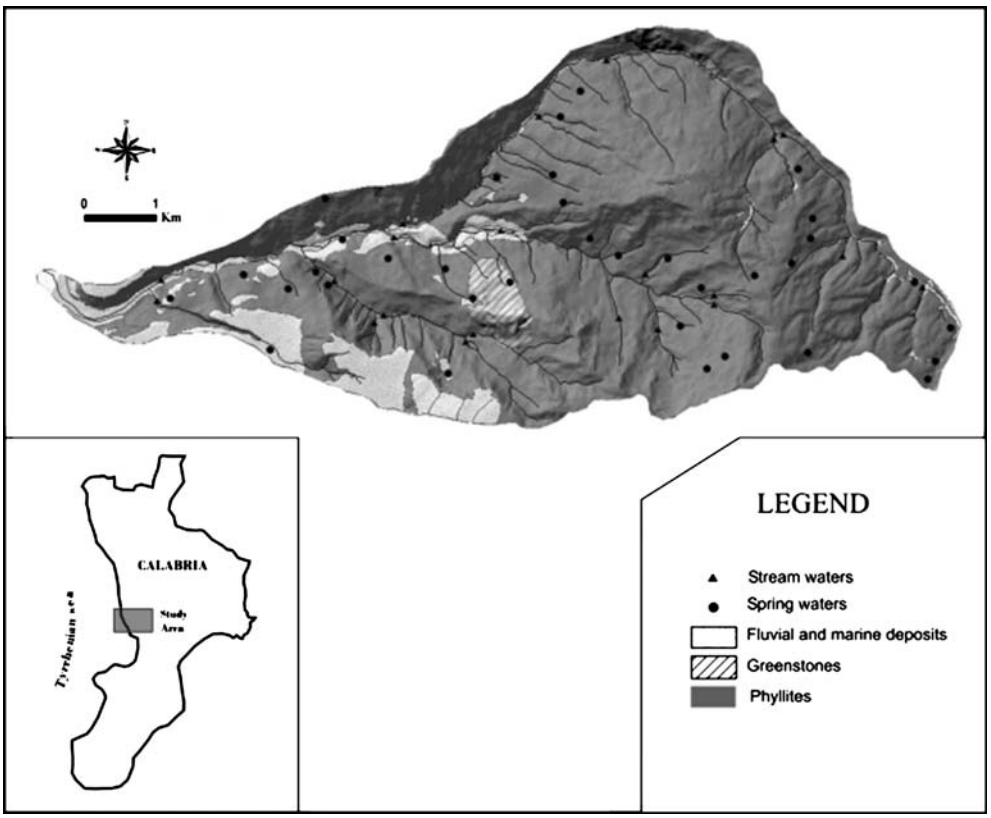

Fig. 1 Geological sketch map of the Fiume Grande catchment. The location of groundwater and stream water samples is also shown

progress (stoichiometric) mode. Stream sediment and soil data are presented and discussed in a companion paper (C. Apollaro et al. in preparation).

Geological background

The phyllitic formation crops out over most of the Fiume Grande valley (Fig. 1). This unit comprises five different lithotypes, namely: phyllites, quartz–phyllites, chlorite–phyllites, carbonate–phyllites, and chloritoid–schists (Piccarretta and Zirpoli 1970).

The main mineralogic constituents of these rocks are: quartz, muscovite (sericite), chlorite, albite, and locally carbonate minerals (chiefly calcite). Accessory minerals are ilmenite, rutile, pyrite, garnet, epidote, tourmaline, and apatite.

In particular, carbonate–phyllites are found in the upper part of the phyllitic formation, together with meta-conglomerates and conglomeratic meta-arkoses. Where carbonate minerals are scarce, they are preferentially found as granoblasts in carbonate–phyllite beds. In contrast, where carbonate minerals are abundant, they form monomineralic levels.

The phyllitic formation is overlain by: (1) the greenstones group, comprising greenschists, glaucophane-schists, quartz-glaucophane-schists, and serpentinites; (2) the group of quartzites and slates. The rocks of these two groups crops out in small sectors of the Fiume Grande valley.

Field operations and laboratory analyses

A total of 22 stream water and 37 spring water samples were collected, in June 2003 and November 2003, respectively, in the Fiume Grande catchment (Fig. 1), which extends over an area of 37 km^2 approximately. Besides, two local rainwaters were also collected and analyzed for major components.

Temperature, electrical conductivity, pH, and Eh were measured in the field. Water was filtered through 0.45 μm cellulose acetate membranes and split in two portions: one was stored in polyethylene bottles without further treatment and the other was acidified through addition of HNO_3 and stored in polyethylene bottles.

Anions were determined by ionic chromatography and alkalinity by acidimetric titration, on the filtered water samples, in the laboratory of the Department of Earth Sciences of the University of Calabria.

Calcium, Mg, Na, K, and Si were measured by ICP-OES and trace elements were determined by ICP-MS, on the filtered-acidified samples, in the laboratory of the Department of Earth Sciences of the University of Cagliari.

All the chemical data are reported in Table 1.

Table 1 Chemical data of stream waters, spring waters, and rainwater of the Fiume Grande catchment

Code	pH	Eh (mV)	T (°C)	Cond (μS/cm)	Ca (ppm)	Mg (ppm)	Na (ppm)	K (ppm)	SO_4 (ppm)	Cl (ppm)	HCO_3 (ppm)	NO_3 (ppm)	F (ppm)	SiO_2 (ppm)	Mn (ppb)	Fe (ppb)	Co (ppb)	Ni (ppm)	Cu (ppb)	Zn (ppb)	As (ppb)
Stream waters																					
F1	6.54	302	14	94.6	10.50	2.78	7.35	0.93	7.11	11.03	39.66	2.46	0.07	5.56	0.57	< 6	0.04	0.45	0.54	1.88	0.49
F2	7.18	293	14	134	15.03	3.58	8.80	1.57	15.05	12.37	51.86	4.59	0.09	6.21	0.42	< 6	0.05	0.53	0.45	< 1.1	0.74
F3	7.37	180.1	15	106	11.76	2.98	8.35	0.80	12.19	12.40	42.71	3.59	0.08	5.99	0.84	< 6	0.04	0.47	< 0.4	1.86	0.65
F4	7.76	213	17	160	18.84	4.71	8.74	1.53	13.70	12.80	57.97	5.95	0.1	5.99	1.66	< 6	0.05	0.59	1.71	2.01	0.68
F5	7.9	185.3	17	208	26.96	7.00	9.61	1.23	20.65	14.43	103.73	4.69	0.11	7.28	0.73	< 6	0.08	1.67	0.83	1.26	1.75
F6	7.37	197.6	20	379	33.61	14.50	29.37	3.39	64.58	37.76	122.03	2.69	0.39	13.91	0.70	< 6	0.07	0.83	1.68	1.48	5.37
F7	8.09	118	21	325	50.65	9.92	11.88	1.48	47.74	16.83	152.54	3.9	0.15	7.92	8.85	< 6	0.08	1.19	0.78	1.23	3.12
F8	8.22	148	21	346	61.83	7.41	12.88	1.19	44.59	17.22	170.85	2.84	0.15	7.70	1.72	< 6	0.08	0.72	0.42	< 1.1	1.14
F9	8.2	258	22	485	65.83	25.05	19.87	2.06	70.46	28.26	247.12	7.42	0.21	9.63	2.84	< 6	0.10	1.14	1.18	2.66	1.09
F10	8.02	220	18	380	60.81	13.57	14.93	1.44	54.98	23.25	195.25	1.38	0.16	8.13	0.53	< 6	0.06	0.86	0.65	1.17	0.95
F11	7.96	236	16	257	41.61	5.69	10.39	0.61	31.19	14.63	125.08	1.54	0.12	7.06	0.55	< 6	0.06	0.71	< 0.4	< 1.1	0.81
F12	7.91	135.4	15	237	40.04	4.36	9.51	0.56	31.00	13.15	122.03	0.96	0.09	5.99	1.83	< 6	0.06	0.55	< 0.4	1.20	0.62
F13	7.87	218	15	274	44.08	6.43	11.99	0.85	30.24	18.08	137.29	4.13	0.13	7.28	0.36	< 6	0.06	0.54	< 0.4	1.23	0.76
F14	7.46	229	12	138	20.96	2.51	8.78	0.65	13.44	11.93	70.17	1.84	0.09	6.42	0.12	< 6	0.04	0.30	< 0.4	< 1.1	0.31
F15	7.63	158.9	15	149	43.39	4.14	10.77	0.65	20.21	14.60	131.19	6.5	0.13	5.99	0.32	< 6	0.07	0.53	0.42	1.27	0.35
F16	7.9	165.5	18	281	46.85	5.94	11.40	0.95	34.32	15.27	134.24	2.36	0.13	6.85	1.40	< 6	0.07	0.63	0.43	4.37	1.26
F17	7.52	274	15	266	24.87	10.06	20.90	0.82	49.41	27.22	85.42	0.57	0.22	14.12	0.30	< 6	0.07	0.55	0.45	3.16	1.91
F18	7.85	184.9	19	449	63.47	17.13	18.91	2.16	64.62	25.78	225.76	13.74	0.17	8.35	0.40	< 6	0.10	1.06	0.50	2.33	0.87
F19	7.96	214	17	301	47.05	7.88	13.10	1.07	25.00	19.62	155.59	2.3	0.16	8.35	1.11	< 6	0.07	0.78	0.42	2.93	0.49
F20	7.72	215	15	208	26.42	7.25	11.84	0.73	21.25	16.96	94.58	1.93	0.13	8.35	0.28	< 6	0.05	0.66	0.45	4.01	1.04
F21	8.37	151.7	26	411	63.10	13.06	16.18	2.85	57.98	21.95	198.30	3.84	0.22	7.70	3.19	< 6	0.10	1.04	0.81	4.22	3.13
F22	8.01	169.6	20	411	65.40	13.12	16.28	2.88	58.17	21.86	195.25	4.35	0.22	8.35	1.61	< 6	0.09	1.17	0.64	6.14	3.12
Spring waters																					
S1	8.09	177	10.2	457	67	15	7.4	0.8	13.02	9.94	236.14	4.24	0.05	7.48	< 3	< 7	0.038	0.5	< 0.3	< 1	8.7
S2	6.27	262	14	167	13	7.2	6.4	2.3	16.70	12.00	40.88	13.56	0.07	8.34	< 3	< 7	0.018	2.2	< 0.3	< 1	< 0.2
S3	6.88	245	10.4	174	24	3.6	6.0	0.3	7.86	9.83	84.20	1.81	0.07	5.77	< 3	< 7	0.021	< 0.3	< 0.3	< 1	0.2
S4	5.57	273	8.9	71.2	2.5	1.8	8.3	0.6	4.31	14.37	9.15	3.77	0.03	7.91	< 3	< 7	0.053	2.7	< 0.3	3	< 0.2
S5	6.88	267	9	121	13	1.8	7.6	0.6	9.73	11.41	34.78	1.29	0.05	5.13	< 3	< 7	0.016	< 0.3	< 0.3	< 1	< 0.2
S6	6.87	237	9	105	9.9	1.6	7.3	0.6	9.14	11.19	30.51	1.16	0.05	5.13	< 3	< 7	0.071	< 0.3	< 0.3	2.8	< 0.2
S7	7.68	210	11.1	236	33	5.5	6.3	1.8	11.67	10.79	105.56	2.65	0.08	7.48	< 3	< 7	0.021	< 0.3	< 0.3	< 1	0.5
S8	8.34	143	13.3	496	78	12	13	0.4	50.12	25.85	217.83	0.69	0.12	10.90	< 3	< 7	0.039	0.6	< 0.3	1.2	< 0.2
S9	7.03	267	14.1	166	12	6.1	9.0	2.6	14.13	18.26	47.59	4.68	0.10	6.63	< 3	< 7	0.021	0.4	< 0.3	3.6	< 0.2
S10	6.64	290	11.3	67.2	2.4	1.8	6.9	0.7	4.46	10.95	9.15	4.72	0.06	10.7	< 3	< 7	0.200	3.1	< 0.3	2.5	< 0.2
S11	6.2	297	11.6	120	8.6	3.8	8.5	0.9	4.55	14.08	35.39	3.99	0.06	14.11	< 3	< 7	0.018	11	< 0.3	1.4	< 0.2
S12	5.96	291	12.5	92.4	7.0	2.4	6.5	0.5	8.18	9.33	25.93	2.69	0.05	7.91	< 3	< 7	0.103	< 0.3	< 0.3	1.6	< 0.2
S13	5.58	334	9.2	50.4	2.1	1.4	5.8	0.7	2.96	11.03	6.71	3.44	0.04	5.77	< 3	< 7	0.197	2.7	< 0.3	2.8	< 0.2
S14	5.72	295	12.4	90.6	6.0	2.1	6.5	1.2	7.35	10.06	16.47	6.04	0.04	6.63	< 3	< 7	0.066	< 0.3	< 0.3	1.7	< 0.2
S15	7.53	213	15.3	362	53	8.2	9.7	0.8	45.17	14.95	150.71	2.58	0.18	6.4	< 3	< 7	0.050	0.3	0.3	2.1	1.4
S16	7.86	216	14.6	410	59	12	11	0.5	22.69	18.95	174.51	8.26	0.09	8.12	< 3	< 7	0.050	0.4	< 0.3	2.5	< 0.2
S17	7.94	234	12.6	410	67	7.9	9.9	1.1	22.73	18.63	196.47	8.24	0.09	8.76	< 3	< 7	0.065	0.4	< 0.3	2.4	< 0.2
S18	6.88	255	16.2	450	42	19	20	3.7	42.66	20.95	167.19	20.42	0.28	12.4	< 3	< 7	0.050	0.8	0.6	4.8	< 0.2
S19	7.69	121	15.5	546	70	14	21	3.3	51.85	34.55	177.56	31.86	0.17	13.04	< 3	< 7	0.060	0.7	< 0.3	2.5	< 0.2
S20	7.5	175	14.1	755	136	11	19	1.2	115.86	33.54	304.47	1.09	0.14	9.41	< 3	< 7	0.096	0.9	< 0.3	2.4	< 0.2
S21	7.71	225	12.2	449	66	12	12	1.4	19.01	21.03	198.92	17.82	0.09	15.61	< 3	< 7	0.034	0.4	0.5	2.5	0.2
S22	7.9	199	13.2	447	76	6.9	10	0.9	22.13	22.48	209.29	6.37	0.12	8.76	< 3	< 7	0.049	0.6	0.6	3.4	< 0.2
S23	7.32	229	15.6	168	8.6	5.0	16	2.9	9.26	14.91	58.58	5.01	0.14	12.62	< 3	39	0.22	< 0.3	0.4	4.4	1.7
S24	7.83	185	14.9	340	33	15	16	1.1	29.01	17.19	147.05	0.10	0.50	23.52	17	< 7	0.045	< 0.3	< 0.3	9.6	14

Table 1 Chemical data of stream waters, spring waters, and rainwater of the Fiume Grande catchment

Code	pH	Eh (mV)	T (°C)	Cond (μS/cm)	Ca (ppm)	Mg (ppm)	Na (ppm)	K (ppm)	SO_4 (ppm)	Cl (ppm)	HCO_3 (ppm)	NO_3 (ppm)	F (ppm)	SiO_2 (ppm)	Mn (ppb)	Fe (ppb)	Co (ppb)	Ni (ppm)	Cu (ppb)	Zn (ppb)	As (ppb)
S25	6.94	180	17.7	233	9.3	7.1	24	1.7	14.94	31.10	49.42	11.58	0.41	27.80	< 3	< 7	0.014	1.4	< 0.3	4.7	2.4
S26	7.66	230	16.8	237	13	7.3	19	1.1	29.58	27.44	40.27	7.04	0.37	23.52	< 3	< 7	0.072	6.0	0.5	7.7	3.4
S27	8.06	203	16	409	29	10	31	5.5	54.43	46.73	60.41	24.81	0.28	21.39	< 3	< 7	0.052	5.5	< 0.3	5.0	1.6
S28	7.46	246	16.6	408	56	7.0	18	0.5	42.24	23.67	159.25	6.58	0.28	15.82	< 3	< 7	0.049	0.7	< 0.3	5.8	0.2
S29	7.25	258	14.4	332	24	14	21	1.1	39.85	30.69	91.53	5.10	0.33	20.10	< 3	< 7	0.028	1.5	< 0.3	5.7	5.8
S30	7.49	278	14.4	374	46	9.5	13	3.3	45.33	21.41	123.56	14.60	0.18	8.98	< 3	< 7	0.34	0.6	< 0.3	15	< 0.2
S31	7.65	230	12.5	380	56	8.1	12	0.7	39.59	20.70	155.59	3.38	0.10	8.34	< 3	< 7	0.15	0.5	< 0.3	9.3	< 0.2
S32	6.82	247	12.1	166	17	4.2	9.7	0.3	15.12	16.60	46.98	4.05	0.10	6.63	< 3	< 7	0.16	0.5	< 0.3	12	1.0
S33	7.22	222	10.9	224	32	3.1	8.4	0.4	25.14	13.07	80.85	1.24	0.08	6.63	< 3	< 7	0.047	0.4	< 0.3	8.7	< 0.2
S34	7.06	230	10.1	155	21	2.0	8.1	0.5	11.35	13.53	61.02	1.86	0.07	6.20	< 3	< 7	0.077	0.3	< 0.3	6	< 0.2
S35	6.83	231	11.5	182	14	5.1	12	0.7	24.30	17.59	37.22	5.56	0.11	11.12	< 3	< 7	0.043	0.7	< 0.3	8.6	2.1

Code	Ca (ppm)	Mg (ppm)	K (ppm)	Na (ppm)	Cl (ppm)	SO_4 (ppm)	HCO_3 (ppm)	NO_3 (ppm)
Rain waters								
R1	0.5	0.7	0.9	6	8.08	3.92	4.37	2.09
R2	0.3	0.1	0.5	0.8	2.03	1	0.93	1.27

Chemical characteristics of stream waters and spring waters

The chemical composition of both stream waters and spring waters is investigated by means of the triangular diagrams of (Na + K)–Ca–Mg and Cl–SO_4–HCO_3, which have been prepared starting from concentrations in eq/L (Fig. 2). Inspection of these plots shows that all the natural waters belong to a unique evolutionary trend from an initial Na–Cl composition, which is typical of rains and some springs, to a late Ca–HCO_3 facies which is exhibited by springs and streams. These compositional changes are accompanied by a variation in salinity from 0.2–0.7 meq/L in rains to 12–17 meq/L in streams and springs, respectively.

The Ca–HCO_3 composition and the low salinity of these waters are typical of relatively limited interaction between meteoric waters and rocks, containing carbonate minerals, such as calcite and dolomite, even in small quantities (Freeze and Cherry 1979). Based on these chemical characteristics, these waters are relatable to shallow, short-lived hydrogeological circuits which are mainly hosted in phyllites containing carbonate minerals.

The correlation plot of P_{CO_2} versus pH (Fig. 3) shows that P_{CO_2} ranges from $10^{-1.5}$ to $10^{-3.5}$ bar in groundwaters and from $10^{-2.0}$ to $10^{-3.1}$ bar in stream waters. Water samples are scattered around the 100 mg HCO_3/L iso-TDIC line, indicating that TDIC varies from some tens to some hundreds mg HCO_3/L.

Groundwaters have average Eh of 234 mV with a minimum of 121 mV and a maximum of 334 mV; stream waters have similar Eh values with an average of 203 mV, a minimum of 118 mV and a maximum of 302 mV.

Average temperature of groundwaters is 13.0 ± 2.5°C (1σ) whereas stream waters have a mean temperature of 17.4 ± 3.3°C.

All these data are needed to constrain geochemical modeling, which represents the subject of the following section.

Reaction path modeling

Reaction path modeling was performed involving the COM thermodynamic database of the EQ3/6 Software Package, version 7.2 (Wolery 1992), after the introduction of minor modifications as discussed by Marini et al. (2001).

In principle, the best way to perform reaction path modeling is in time frame (or kinetic reaction progress mode), that is specifying surface areas and rates of dissolution–precipitation for relevant mineral phases. However, the surface areas of mineral phases in natural systems are very difficult to be defined (e.g., Lichtner

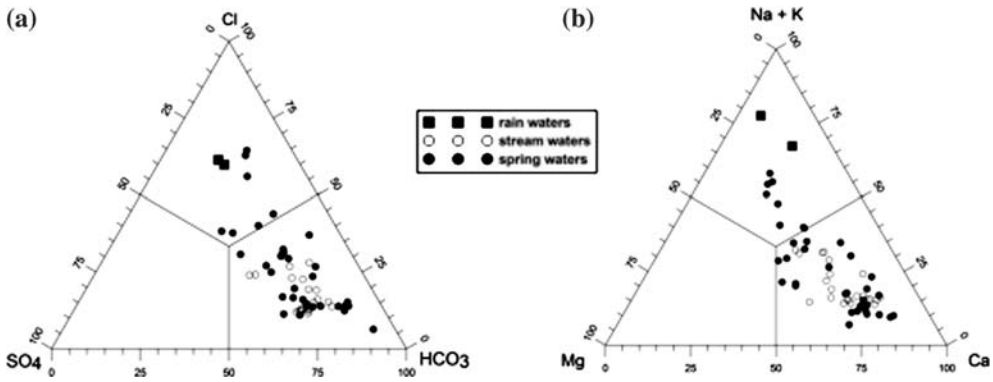

Fig. 2 Triangular diagrams of **a** $Cl–SO_4–HCO_3$ and **b** (Na + K)–Ca–Mg, prepared starting from concentrations in equivalent units, for the stream waters, spring waters, and rain waters of the Fiume Grande catchment

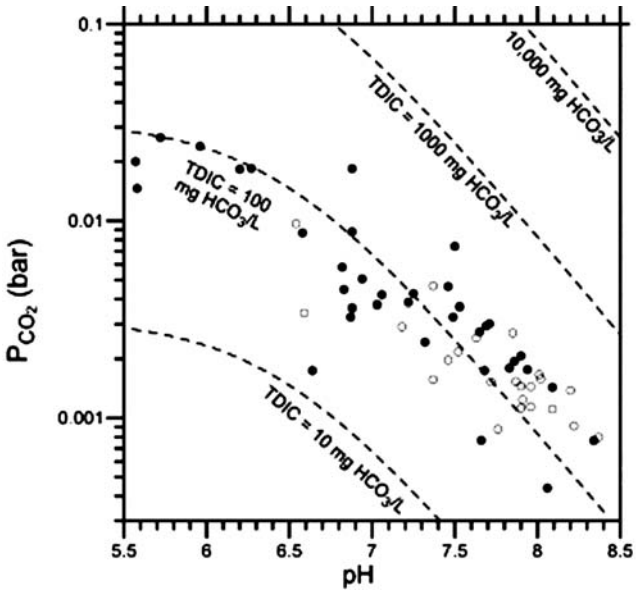

Fig. 3 Correlation plot of P_{CO_2} versus pH for the stream waters (*open circles*) and spring waters (*closed circles*) of the Fiume Grande catchment

1996, 1998; Appelo and Postma 1999), deviate strongly from the surface area in laboratory experiments of mineral dissolution/precipitation, and change dramatically during progressive water–rock interaction owing to different, sometimes contrasting effects (White and Brantley 2003). Besides, close-to-equilibrium field rates are lower than far-from-equilibrium laboratory rates (White and Brantley 2003). Owing to these difficulties, we decided to perform reaction path modeling referring to the reaction progress variable, ξ, that is through a purely stoichiometric approach that does not take into account the kinetics of irreversible water–rock mass exchanges. In other terms, in this way there is no need to guess neither surface areas nor dissolution/precipitation rates.

The solid reactants

A further advantage of the stoichiometric approach is that whatever material of known stoichiometry, irrespective of its thermodynamic stability, e.g. a rock, can be taken as reactant. A complication arising from the geological setting of the study area is the local presence of a relatively fast dissolving carbonate mineral, i.e., calcite, in phyllitic rocks, whose major mineralogic constituents (quartz, muscovite, chlorite, and albite) dissolve much slower than calcite. To circumvent this problem, two solid reactants were involved in the simulation: (1) a phyllitic rock, which was treated as a special reactant, in the EQ3/6 terminology (Wolery and Daveler 1992) and (2) calcite, which was considered to be a pure mineral. Both solid reactants were assumed to dissolve at the same relative rate to balance the comparatively high dissolution rate and low abundance of calcite with the low dissolution rate and high abundance of silicate minerals constituting the phyllitic rock.

Table 2 Chemical composition of the local phyllite considered in reaction path modeling

SiO_2 (wt %)	Al_2O_3 (wt %)	TiO_2 (wt %)	Fe_2O_3 (wt %)	MnO (wt %)	CaO (wt %)	MgO (wt %)	Na_2O (wt %)	K_2O (wt %)	P_2O_5 (wt %)
63.40	16.78	0.69	6.11	0.08	0.83	3.11	1.74	2.83	0.09

V (ppm)	Cr (ppm)	Co (ppm)	Ni (ppm)	Zn (ppm)	As (ppm)	Y (ppm)	Zr (ppm)	Nb (ppm)	Sr (ppm)	Ba (ppm)	Rb (ppm)	Pb (ppm)
123.4	99	18.2	43.4	69.4	7.2	28.2	184.4	13.2	68.6	420.8	113.4	12.2

The local phyllitic rock (Table 2) was introduced in the EQ6 input file after recalculating its composition on an elemental basis. During progressive dissolution of the latter reactant, its composition was eventually changed subtracting the contribution of the primary minerals with which the aqueous solution attained equilibrium (saturation), namely muscovite, albite, and clinochlore. These corrections were done considering the stoichiometric composition of these pure minerals, whereas the trace element contents of the phyllitic rock were not changed. These corrections were needed only in the simulations in which P_{CO_2} was fixed at 10^{-3} and $10^{-3.5}$ bar (see below).

Simulations were performed in titration mode. In other words, at each step of ξ, corresponding amounts of the two solid reactants are added to the considering system, including the aqueous solution and any secondary phases. The added reactants are dissolved and resulting secondary phases, if any, are re-equilibrated with the aqueous solution (Wolery and Daveler 1992).

Infiltrating rainwater

The average Cl content of infiltrating rainwater, eventually concentrated through evapotranspiration, was assumed to be 19 mg/L, which is equal to the mean Cl content of sampled springs and stream waters.

Since rainwaters in near-coastal areas, such as the Fiume Grande catchment, can be considered strongly diluted marine waters (Appelo and Postma 1999; Berner and Berner 1996), concentrations of all the considered chemical constituents in rainwater, $C_{i,R}$, were computed as follows:

$$C_{i,R} = C_{i,S}\left(\frac{C_{Cl,R}}{C_{Cl,S}}\right), \quad (1)$$

where $C_{i,S}$ is the average seawater content of the i-th chemical constituent (taken from the file SWTST.3i of the EQ3/6 software package) and $C_{Cl,R}$ and $C_{Cl,S}$ are the average Cl content of rainwater and seawater, respectively.

Total dissolved inorganic carbon concentration was fixed by the electro-neutrality condition in running EQ3 and a P_{CO_2} of $10^{-3.5}$ bar, i.e., the average atmospheric value, was assumed to constrain pH. The composition of infiltrating rainwater is given in Table 3.

Table 3 Chemical composition of the infiltrating rainwater considered in reaction path modeling (T = 13°C, pH = 5.5)

Element	Ppm
Ca	0.405
Mg	1.27
Na	10.6
K	0.392
SO_4	2.66
Cl	19
TDIC (as HCO_3)	10.12
NO_3	2.85E-04
NH_3	2.78E-05
SiO_2	0.0042
Al	1.96E-06
Mn	1.96E-07
Fe	1.96E-06
Co	4.91E-08
Ni	1.67E-06
Zn	4.81E-06
H_2AsO_4	7.39E-06

The T- P_{CO_2}– f_{O_2} conditions

Different runs were performed interacting the two solid reactants (the local phyllite and calcite) with rainwater at constant temperature, 13°C, and f_{O_2}, $10^{-41.6}$ bar, closely corresponding to the average values of local springs (see above), whereas P_{CO_2} was taken equal to $10^{-1.5}$, $10^{-2.0}$, $10^{-2.5}$, $10^{-3.0}$ and $10^{-3.5}$ bar, to evaluate the influence of this variable. These P_{CO_2} values span the range of local natural waters (see above). Moreover, $10^{-1.5}$ bar is the maximum value for a normal soil (Brook et al. 1983).

The possible product solid phases

The selection of secondary (product) solid phases generated during progressive dissolution of phyllite plus calcite in meteoric water is not unique. In fact, different selections may lead to reproduce satisfactorily the chemical composition of local natural waters. Hints on the product phases possibly produced during the process of interest are given both by the present understanding of chemical weathering (e.g., Berner and Berner 1996; Langmuir 1997; Appelo and Postma 1999) and by relevant activity plots in which local natural waters are reported (e.g., Fig. 4). These plots suggest that gibbsite, kaolinite, and beidellites may be formed during the evolution of the natural waters of the Fiume Grande catchments, whereas saturation with amorphous silica and calcite (or, in general, a trigonal carbonate solid mixture) represents effective geochemical barriers.

Based on these considerations, to avoid the formation of undesired minerals (which are unlikely to be produced under the low-temperature, low-pressure conditions prevailing in the surface network and in shallow hydrologic circuits), and to maintain reaction path modeling to a relatively simple level, only gibbsite, kaolinite, amorphous silica, illite [$K_{0.6}Mg_{0.25}Al_{1.8}Al_{0.5}Si_{3.5}O_{10}(OH)_2$], a smectite solid mixture made up of Na- and K-beidellite [$(K,Na)_{0.33}Al_{2.33}Si_{3.67}O_{10}(OH)_2$,], a hydroxide solid mixture [constituted by $Fe(OH)_3$, $Cr(OH)_3$, $Mn(OH)_3$, $Fe(OH)_2$, $Mn(OH)_2$, $Co(OH)_2$, $Ni(OH)_2$, $Zn(OH)_2$] and a trigonal carbonate solid mixture (made up of calcite,

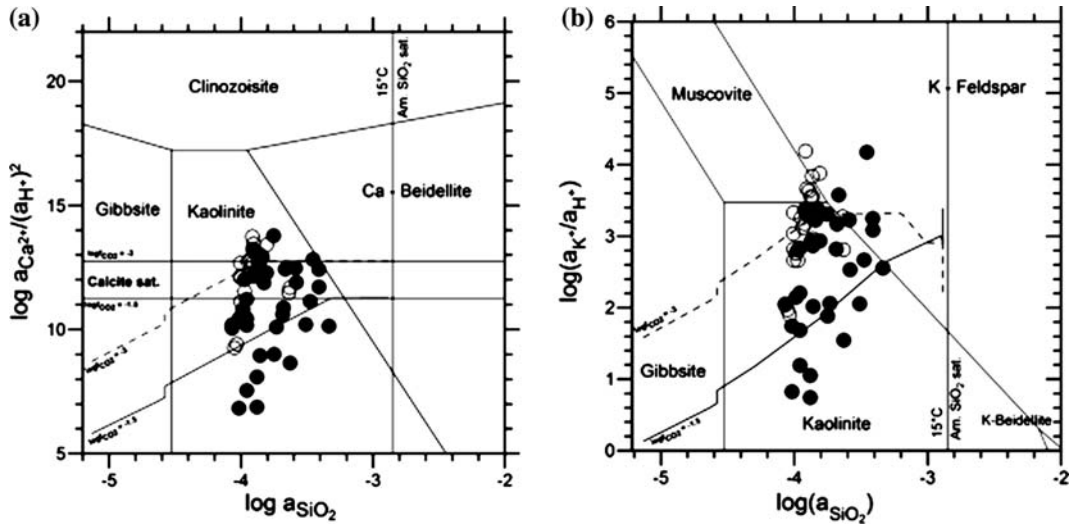

Fig. 4 Activity plots for the systems **a** $CaO–SiO_2–Al_2O_3–H_2O$ and **b** $K_2O–SiO_2–Al_2O_3–H_2O$ reporting the stream waters (*open circles*) and spring waters (*closed circles*) of the Fiume Grande catchment, as well as the theoretical trends obtained by means of the EQ6 simulations at temperature of 13°C, f_{O_2} of $10^{-41.6}$ bar, and P_{CO_2} of 10^{-3} bar and $10^{-1.5}$ bar

rhodochrosite, siderite, sphaerocobaltite, gaspeite, and smithsonite) were allowed to be generated as secondary phases[1]. Solid mixtures were assumed to be ideal, as this is the only mixing model at the solid state supported by the used version of the EQ3/6 software package. Their compositions vary with ξ (see below). See Marini et al. (2001) for further details.

It must be noted that the choice of secondary solid phases is a very delicate point in reaction path modeling as the aqueous solution, after the initial stage of congruent dissolution of solid Al–silicate reactants, attains equilibrium with product minerals, whereas primary reactants act only as suppliers of chemical elements. Therefore the composition of primary reactants chiefly constrain the amount of solid product phases rather than the composition of the aqueous solution, of course during the relatively late stage of incongruent dissolution of solid Al–silicate reactants.

Results of reaction path modeling: the product solid phases

The molar amounts of secondary solid phases produced through progressive dissolution of phyllite plus calcite under a fixed P_{CO_2} of 10^{-3} and $10^{-1.5}$ bar are shown as a function of the reaction progress variable and pH in Fig. 5. Results obtained at different P_{CO_2} values are relatively similar and are not shown for space reasons. Gibbsite, the hydroxide solid mixture, and kaolinite are early appearing product phases in all the simulations, independent of P_{CO_2}, whereas the carbonate solid mixture, the beidellite solid mixture, amorphous silica, and illite are produced at higher values ofξ and pH.

Gibbsite and kaolinite have ephemeral existence at all the P_{CO_2} values. Illite has a similar behavior at P_{CO_2} of 10^{-3} and $10^{-3.5}$ bar, but it becomes a persistent mineral at higher P_{CO_2} values. The hydroxide solid mixture, the carbonate solid mixture, the beidellite solid mixture, and amorphous silica are persistent solid phases at any P_{CO_2} value and are generated in comparatively high amounts. Gibbsite and kaolinite are produced in relatively small amounts, whereas the moles of illite depend markedly on P_{CO_2}.

Carbon dioxide partial pressure has a significant influence on the ξ values of first appearance of product phases for all these minerals except kaolinite. The lower the P_{CO_2}, theearlier all the secondary phases begin to precipitate.

The composition of the beidellite solid mixture depends markedly on P_{CO_2}. At P_{CO_2} of 10^{-3} and $10^{-3.5}$ bar the aqueous solution saturates relatively early with muscovite, whose dissolution is inhibited at higher ξ values. Consequently, the system remains relatively poor of K and the beidellite solid mixture enriches in the Na-component, with molar fractions higher than 0.9. In contrast, for $P_{CO_2} \geq 10^{-2.5}$ bar, the aqueous solution remains undersaturated with muscovite, whose continuous dissolution supplies K to the system triggering precipitation of a K-rich, Na-poor beidellite. At high P_{CO_2} values, illite precipitation brings about a minor inflection in the molar fraction of K-beidellite.

[1]The term "solid solution" is generally preferred to "solid mixture" in the geochemical literature. However in a solution it is possible to distinguish the solvent from the solute(s), which is not the case for the "solid solutions". These should be called, therefore, "solid mixtures".

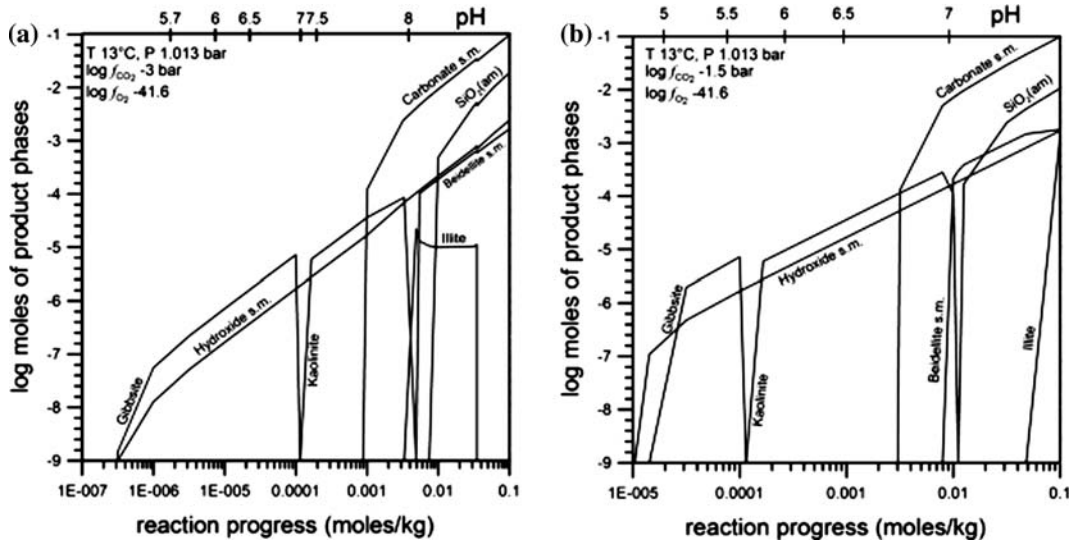

Fig. 5 Moles of secondary mineral phases produced through progressive dissolution of phyllite plus calcite at temperature of 13°C, f_{O_2} of $10^{-41.6}$ bar, and P_{CO_2} of **a** 10^{-3} bar and **b** $10^{-1.5}$ bar. The pH scale is shown for reference

The hydroxide solid mixture (Fig. 6) is constituted by almost pure Fe(III) hydroxide, with minor amounts of Cr hydroxide ($0.0001 < X_{Cr(OH)3} < 0.003$) and even smaller contents of $Ni(OH)_2$, $Zn(OH)_2$, $Co(OH)_2$, and (at low P_{CO_2} values) $Mn(OH)_2$. The molar fractions of these divalent-metals hydroxides generally increase with the reaction progress.

Fig. 6 Compositions of the hydroxide solid mixture precipitating during progressive dissolution of phyllite plus calcite at temperature of 13°C, f_{O_2} of $10^{-41.6}$ bar, and P_{CO_2} of **a** 10^{-3} bar and **b** $10^{-1.5}$ bar. The pH scale is shown for reference

In the solid mixture of trigonal carbonates (Fig. 7), calcite is the main component at all P_{CO_2} and ξ values, with molar fractions close to 1. In general, as already recognized by Marini et al. (2001), the molar fractions of the carbonate minerals less soluble than calcite (e.g., rhodochrosite and smithsonite) decrease with increasing ξ, the content of gaspeite, which is more soluble than calcite, increase with ξ, whereas the molar fraction of siderite remains constant at 4.1×10^{-7} for any value of ξ.

Owing to dissolution of calcite and precipitation of a solid mixture of trigonal carbonates, which is largely made up of calcite, the geochemical model is very close to a limiting, inconsistent condition in which the same mineral is both dissolved and precipitated. In terms of energy, the "distance" from this limiting condition is given by the

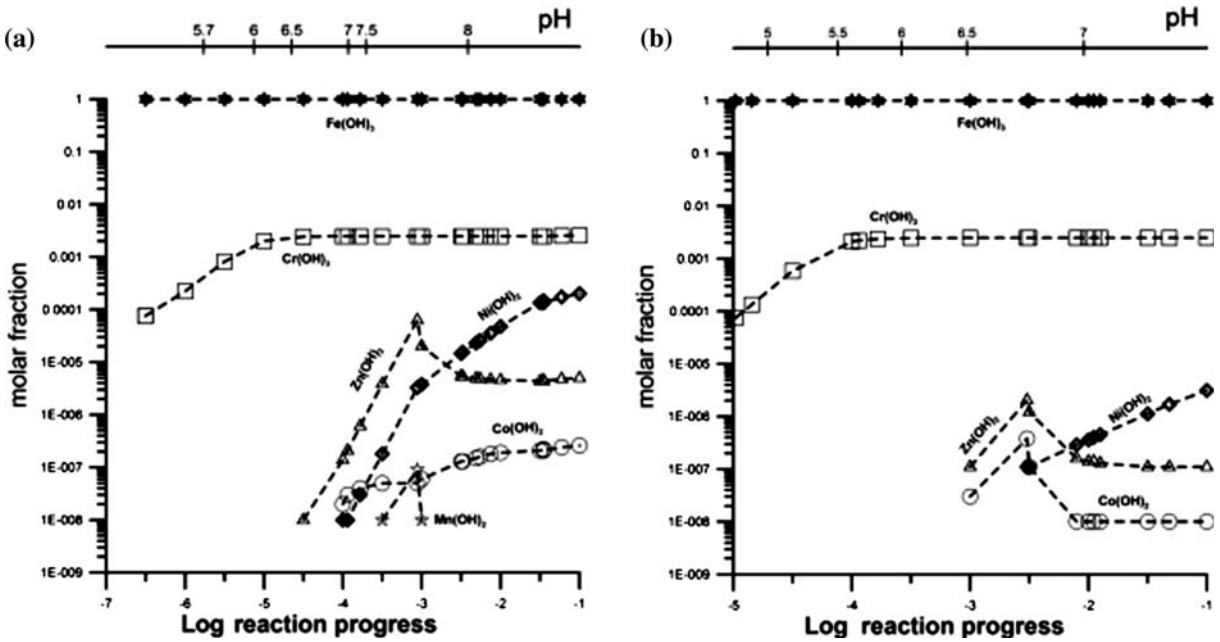

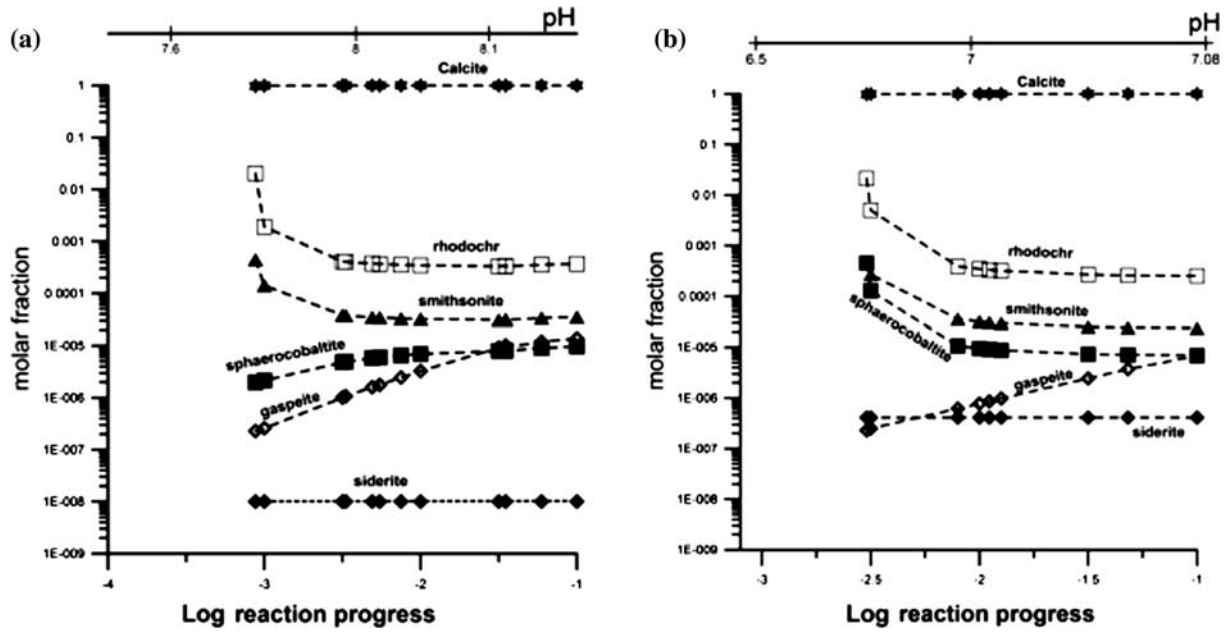

Fig. 7 Compositions of the solid mixture of trigonal carbonates precipitating during progressive dissolution of phyllite plus calcite at temperature of 13°C, f_{O_2} of $10^{-41.6}$ bar, and P_{CO_2} of **a** 10^{-3} bar and **b** $10^{-1.5}$ bar. The pH scale is shown for reference

Gibbs free energy of ideal mixing, which stabilizes the ideal solid mixture with respect to the component minerals. The Gibbs free energy of ideal mixing is obtained by means of the relation (e.g., Ottonello 1997):

$$G_{\text{ideal mixing}} = RT\sum_i X_i \cdot \ln X_i, \qquad (2)$$

where X_i is the molar fraction of the the i-th mineral component, R is the universal gas constant, and T is the temperature (in Kelvin). Inserting the molar fractions of calcite, rhodochrosite, siderite, sphaerocobaltite, gaspeite, and smithsonite computed by EQ6, it turns out that $G_{\text{ideal mixing}}$ varies from −66 to −2 cal/mole. These are very small figures, but they are enough to make the model consistent.

The incorporation of trace elements in these precipitating solid mixtures, especially in trigonal carbonates, has a marked influence on the composition of the aqueous solution, which is the subject of the next section.

Results of reaction path modeling: the dissolved constituents

In this section, log(concentration) versus pH correlation plots are used to compare the total contents of aqueous constituents predicted by reaction path modeling with the corresponding analytical data (Figs. 8, 9, 10). The pH is selected as reference variable, since water–rock interaction is a sort of acid–base titration, in which the carbonate and silicate minerals act as bases and dissolved CO_2 represents the main acid. This titration gradually shifts the pH of the aqueous solution from the initial, slightly acidic values (4.5–6 in this case), which are controlled by the P_{CO_2} of the system, to the final, slightly basic values (7–8.5), which are constrained (according to the EQ3/6 simulation) by saturation with the trigonal carbonate phase under P_{CO_2} of $10^{-1.5}$–$10^{-3.5}$ bar. Since chemical constituents experience, during this process, changes in concentration of several orders of magnitude, the logarithmic scale was used instead of the linear scale for the preparation of the plots of Figs. 8, 9, and 10.

The analytical concentrations of the major dissolved constituents typically controlled by water–rock interaction (Ca, Mg, Na, K, TDIC, SiO_2) and some trace elements (Mn, Co, Ni, Zn, and As) are reproduced satisfactorily by reaction path modeling. Among these constituents, only TDIC, Ca, Mn, Co, and As are presented in detail below, for space reasons.

TDIC At low pH values ($\ll$6.5), theoretical concentrations of total dissolved inorganic carbon are nearly pH independent, as TDIC concentration is practically equal to the content of aqueous CO_2, which is fixed by P_{CO_2} (Fig. 8a). At pH close to 6.5 (which is equal to $-pK_{CO_2(aq)}$ at the considered temperature of 13°C), the trend bends upwards, as $a_{CO_2(aq)} = a_{HCO_3^-}$. Upon further water–rock interaction, TDIC concentration becomes practically equal to the HCO_3 content and, therefore, log(TDIC) increases with pH approaching a straight line of slope +1. A similar trend was observed for groundwaters interacting with calcite and dolomite (Langmuir 1971).

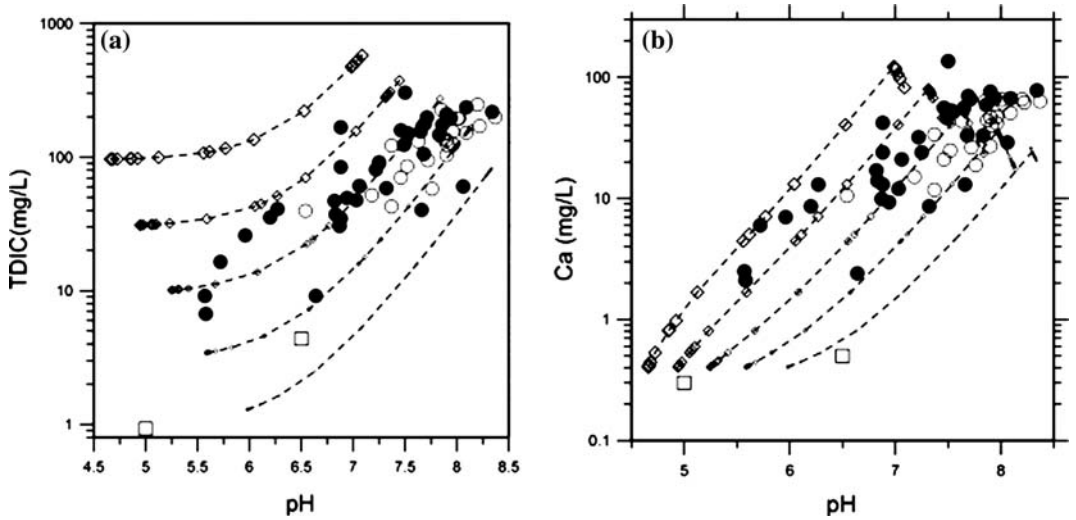

Fig. 8 Plots of **a** total dissolved inorganic carbon (*TDIC*) versus pH and **b** total dissolved Ca versus pH showing both analytical data (*closed circles* springs, *open circles* streams, *open squares* rains) and the results of reaction path modeling, carried out at fixed temperature of 13°C and f_{O_2} of $10^{-41.6}$ bar, and variable P_{CO_2}, from $10^{-1.5}$ bar (*largest open diamonds*) to $10^{-3.5}$ bar (*smallest open diamonds*) at steps of half log unit

Theoretical TDIC and corresponding pH values outline different paths, which are equally spaced of half log-unit along the vertical axis, as they correspond to P_{CO_2} values differing by 0.5 log-units.

Upon attainment of saturation with respect to the trigonal carbonate solid mixture, only minor changes of calculated TDIC and pH are observed, at constant P_{CO_2}. Theoretical TDIC and pH, calculated for different P_{CO_2} values, plot close to a straight line of slope −0.5, as observed for groundwaters approaching equilibrium with calcite (Langmuir 1971).

As expected based on Fig. 3 and related observations, most analytical data distribute in Fig. 8a around the theoretical line for P_{CO_2} of $10^{-2.5}$ bar and are limited by the theoretical lines for P_{CO_2} of 10^{-2} and 10^{-3} bar. Most stream waters and about 50% of the springs either approach saturation with respect to the trigonal carbonate solid mixture or are slightly oversaturated.

It must be underscored that the theoretical paths calculated for fixed P_{CO_2} and temperature are a simplified approximation of complex natural phenomena. It is unlikely that each natural water moves along a given theoretical path for a fixed P_{CO_2} value under open-system conditions with respect to CO_2. Meteoric waters, during their evolution towards the saturation with the trigonal carbonate solid mixture, likely jump between different CO_2-buffered conditions or even evolve under closed-system conditions.

Calcium Similar to what observed for the late, linear theoretical evolution of TDIC (see above), the logarithms of theoretical total Ca concentrations and corresponding pH values plot along different lines of slope close to +1, equally spaced of half log-unit along the vertical axis, since they correspond to P_{CO_2} values differing by 0.5 log-units (Fig. 8b). Again, upon attainment of saturation with the trigonal carbonate solid mixture, only slight changes in Ca concentration and pH occur at constant P_{CO_2}, while theoretical values for distinct P_{CO_2} values plot close to a straight line of slope −0.5 (Langmuir 1971).

As observed for TDIC, most streams and about 50% of the springs have analytical Ca contents and pH values either consistent with the attainment of saturation with the trigonal carbonate solid mixture or somewhat higher. Although reaction path modeling cannot reproduce oversaturation, a slight oversaturation is not uncommon in natural waters discharged by carbonate-bearing aquifers, owing to the slow precipitation rates of calcite for saturation indexes lower than 0.3 (Appelo and Postma 1999).

Manganese and cobalt The theoretical concentrations of Mn and Co increase quite regularly with pH before attainment of saturation with respect to the trigonal carbonate solid mixture. (Fig. 9) and the influence of P_{CO_2} on the reaction path is nil prior to the onset of carbonate precipitation. When the trigonal carbonate solid mixture begins to precipitate, the theoretical concentrations of dissolved Co (at high P_{CO_2} values) and Mn (at all the P_{CO_2} values) experience a marked decrease as the free ions Co^{2+} and Mn^{2+} are preferentially incorporated in the precipitating solid phase. This behavior is consistent with the lower solubilities of sphaerocobaltite and rhodochrosite with respect to calcite. In contrast, at low P_{CO_2} values, dissolved Co content continues to increase as it is supplied to the system by rock dissolution but it is evidently not removed by the precipitating carbonate.

The different evolutions of dissolved Mn and Co are explained by their different speciation in the aqueous solutions. Indeed, the free ion Mn^{2+} is the prevailing

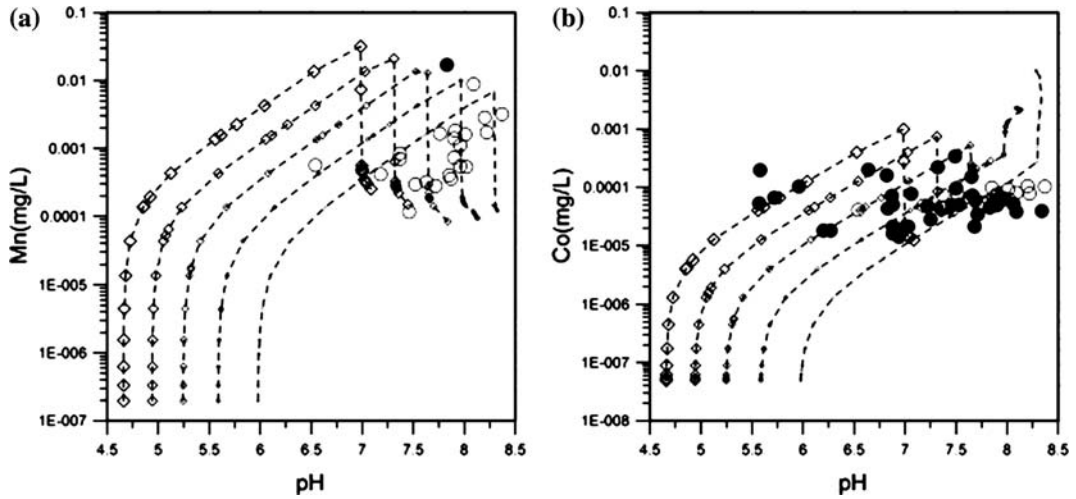

Fig. 9 Plots of **a** total dissolved Mn versus pH and **b** total dissolved Co versus pH showing both analytical data (*closed circles* springs, *open circles* streams) and the results of reaction path modeling, carried out at fixed temperature of 13°C and f_{O_2} of $10^{-41.6}$ bar, and variable P_{CO_2},, from $10^{-1.5}$ bar (*largest open diamonds*) to $10^{-3.5}$ bar (*smallest open diamonds*) at steps of half log unit

dissolved species of Mn at all pH and P_{CO_2} values, whereas the dominant aqueous species of Co are either the free ion Co^{2+} below pH 7.1 or the complex species $HCoO_2^-$ above this pH threshold. In other words, in the pH range of carbonate precipitation, the major dissolved species of Co are either the free ion Co^{2+}, at P_{CO_2} of $10^{-1.5}$, $10^{-2.0}$, and $10^{-2.5}$ bar, or the complex species $HCoO_2^-$ at P_{CO_2} of 10^{-3} and $10^{-3.5}$ bar.

It must be noted that the COM database of EQ3/6 reports a log K of 21.2430 at 25°C (from Wagman et al. 1982) for the dissociation reaction:

$$HCoO_2^- + 3H^+ = Co^{2+} + 2H_2O, \quad (3)$$

but the influence of temperature on the log K of reaction (3) is unknown. It is therefore likely that the pH of $Co^{2+}/HCoO_2^-$ isoactivity deviates somewhat from 7.1 at the temperature of interest (13°C), although the correct value is unknown. In spite of these uncertainties, reaction path modeling provides a consistent framework for the interpretation of analytical Mn and Co data of streams and springs, which agree in general with the theoretical trends.

Arsenic The total concentration of dissolved As increases regularly with ξ throughout the simulations as it is continuously supplied to the aqueous solution by rock dissolution and it does not enter any secondary solid phases. In contrast, the theoretical evolution of As with pH is characterized by a first part (for pH values lower than those of saturation with the solid mixture of trigonal carbonates), in which both parameters increase together, and by a second part (above these pH thresholds), in which dissolved As continues to increases at nearly constant pH, as pH is controlled by saturation with the solid mixture of trigonal carbonates at constant P_{CO_2} (Fig. 10). Analytical As concentrations are in good agreement with the theoretical trends.

According to the EQ3/6 simulations, under the comparatively oxidising conditions imposed to the model, As is present at the pentavalent state and the main dissolved species are the $H_2AsO_4^-$ ion below pH 6.79 and the $HAsO_4^{2-}$ ion above pH 6.79, which is the log K of the reaction:

$$HAsO_4^{2-} + H^+ = H_2AsO_4^- \quad (4)$$

at the temperature of interest.

Accepting both this indication and the occurrence of Fe(III) hydroxide precipitation through most of the simulation (see above), As is expected to be entirely sorbed on this solid phase at pH lower than ~ 12 (Dzomback and Morel 1990). If so, the expected contents of dissolved As would be much lower than analytical values. A possible way to reconcile these theoretical expectations with analytical data is to hypothesize the occurrence of complexation reactions between $H_2AsO_4^-$ or $HAsO_4^{2-}$ ions and presently unknown cations with formation of either neutral or positively charged complexes. Neutral complexes are not sorbed by Fe(III) hydroxide whereas positively charged complexes are expected to behave as free cations, which exhibit low sorption edges (i.e., the pH at which 50% of the sorbate has been sorbed) and an increase in sorption with pH (Stumm 1992). A similar behavior was found for Cr(VI), in mixtures of acid waters from the derelict Libiola mine (Italy) and stream waters, owing to the formation of the neutral $CuCrO_4°$ aqueous complex (Accornero et al. 2005).

Unfortunately the stability constants of arsenate complexes are not well known at present. Values for the 1:1 metal-arsenate complexes involving $H_2AsO_4^-$,

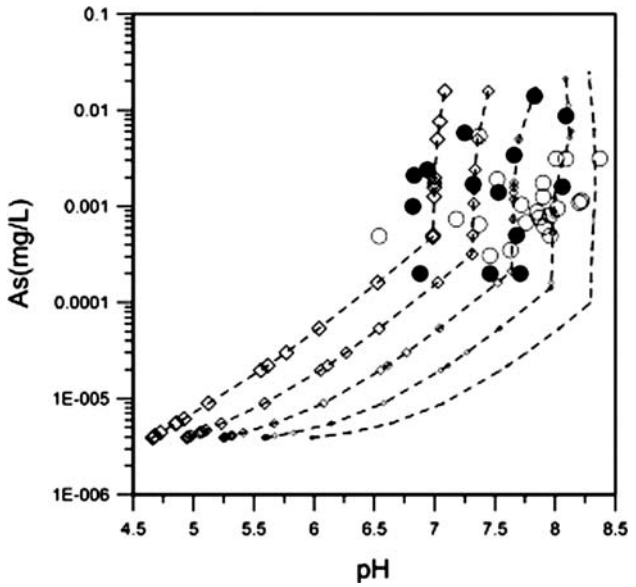

Fig. 10 Plot of total dissolved As versus pH showing both analytical data (*closed circles* springs, *open circles* streams) and the results of reaction path modeling, carried out at fixed temperature of 13°C and f_{O_2} of $10^{-41.6}$ bar, and variable P_{CO_2}, from $10^{-1.5}$ bar (*largest open diamonds*) to $10^{-3.5}$ bar (*smallest open diamonds*) at steps of half log unit

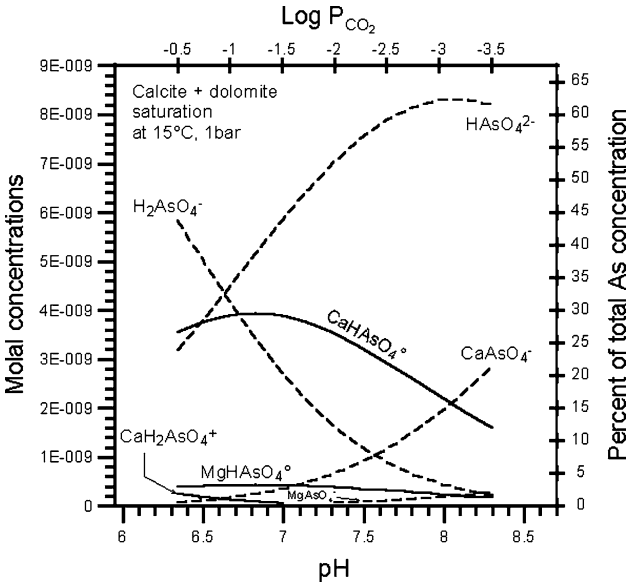

Fig. 11 Speciation of dissolved arsenate in an aqueous solution in equilibrium with calcite and dolomite, at 15°C, 1 bar total pressure, under variable P_{CO_2}, from $10^{-0.5}$ to $10^{-3.5}$ bar

$HAsO_4^{2-}$, and AsO_4^{3-} ions and Mg^{2+}, Ca^{2+}, Al^{3+}, and some transition metals, at 25°C, 1 bar are reported by Langmuir et al. (1999; from Whiting 1992). The values for the Mg- and Ca-arsenate complexes were inserted in the EQ3/6 thermodynamic database to compute the speciation of dissolved arsenate for an aqueous solution in equilibrium with calcite and dolomite under variable P_{CO_2}, from $10^{-0.5}$ to $10^{-3.5}$ bar, representing a proxy for the natural waters of the study area. Results (Fig. 11) suggests that the neutral complexes $CaHAsO_4°$ and $MgHAsO_4°$ represent together up to 33% of dissolved As, in spite of the prevalence of anionic species (> 66%), whereas cationic species (e.g., $CaH_2AsO_4^+$) are negligible under these conditions. Further researches on the complexation between As(V)-anions and cations are needed to clarify this matter.

Conclusions

The irreversible water–rock mass exchanges occurring during the evolution of rainwaters to stream waters and groundwaters of the Fiume Grande valley were simulated through reaction path modeling in reaction progress (stoichiometric) mode. Two reactants were involved in the simulation, namely a phyllitic rock and calcite, and they were assumed to dissolve at the same relative rate to compensate the relatively high dissolution rate and low amounts of calcite with the low dissolution rate and high amounts of silicate minerals constituting the phyllite.

Different runs were carried out at constant temperature, 13°C, and f_{O_2}, $10^{-41.6}$ bar, reproducing the mean values of local springs, whereas P_{CO_2} was fixed at $10^{-1.5}$, $10^{-2.0}$, $10^{-2.5}$, $10^{-3.0}$ and $10^{-3.5}$ bar, to span the range of local natural waters.

Based on the general understanding of chemical weathering and the indication provided by activity plots, only gibbsite, kaolinite, amorphous silica, illite, a smectite solid mixture, a hydroxide solid mixture, and a trigonal carbonate solid mixture were allowed to precipitate as secondary (product) solid phases.

Results of reaction path modeling reproduce satisfactorily the analytical concentrations of major and trace elements in stream waters and groundwaters. Besides, the role played by the trigonal carbonate solid mixture (which is chiefly made up of calcite) as sequestrator of some trace elements (e.g., Mn and Co) is emphasized, in line with previous findings (Rimstidt et al. 1998; Marini et al. 2001).

Also analytical As concentrations agree with theoretical values. However, accepting that (1) the main dissolved As species are either the $H_2AsO_4^-$ ion or the $HAsO_4^{2-}$ ion, depending on pH, and (2) Fe(III) hydroxide precipitates through most of the simulation, as indicated by reaction path modeling, then As is expected to be wholly sorbed onto this solid (Dzomback and Morel 1990). If so, the analytical contents of dissolved As would be much lower than the expected values. This suggests

occurrence of complexation reactions between $H_2AsO_4^-$ or $HAsO_4^{2-}$ ions and presently unknown cations with formation of either neutral or positively charged complexes. Further investigations are necessary to clarify this matter.

Acknowledgments This research was supported by a Ph.D. fellowship and research funds from the University of Calabria. The authors wish to thank Rosa Cidu and Riccardo Biddau of the Department of Earth Sciences of the University of Cagliari for the analytical support.

References

Accornero M, Marini L, Ottonello G, Vetuschi Zuccolini M (2005) The fate of major constituents and chromium and other trace elements when acid waters from the derelict Libiola mine (Italy) are mixed with stream waters. Appl Geochem 20:1368–1390

Apollaro C, De Rosa R, Ferruzza G (2003) The Cosenza and Messina sheets of the geochemical map of Italy: explanatory notes. In: Ottonello G, Serva L (eds) Geochemical baselines of Italy. Pacini, Pisa, pp 287–294

Apollaro C (2005) Geochemical characteristics of rocks, stream sediments, soils, and waters of the Fiume Grande catchment (CZ) and water–rock interaction modeling (in Italian). PhD, University of Calabria, Italy

Appelo CAJ, Postma D (1999) Geochemistry, groundwaters and pollution. A.A. Balkema, Rotterdam

Berner EK, Berner RA (1996) Global environment: water, air, and geochemical cycles. Prentice Hall, Upper Saddle River

Brook GA, Folkoff ME, Box EO (1983) A world model of soil carbon dioxide. Earth Surf Proc 8:79–88

Dzombak DA, Morel FMM (1990) Surface complexation modelling, hydrous ferric oxide. Wiley, New York

Freeze RA, Cherry JA (1979) Groundwater. Prentice Hall, Upper Saddle River

Langmuir D (1971) The geochemistry of some carbonate ground waters in central Pennsylvania. Geochim Cosmochim Acta 35:1023–1045

Langmuir D (1997) Aqueous environmental geochemistry. Prentice Hall, Upper Saddle River

Langmuir D, Mahoney J, MacDonald A, Rowson J (1999) Predicting arsenic concentrations in the porewaters of buried uranium mill tailings. Geochim Cosmochim Acta 63:3379–3394

Lichtner PC (1996) Continuum formulation of multicomponent-multiphase reactive transport. In: Lichtner PC, Steefel CI, Oelkers EH (eds) Reactive transport in porous media. Rev Mineral 34:1–81

Lichtner PC (1998) Modeling reactive flow and transport in natural systems. In: Marini L, Ottonello G (eds) Proceedings of the Rome seminar on environmental geochemistry, Pacini, Pisa, pp 5–72

Marini L, Canepa M, Cipolli F, Ottonello G, Vetuschi Zuccolini M (2001) Use of stream sediment chemistry to predict trace element chemistry of groundwater, a case study from the Bisagno valley (Genoa, Italy). J Hydrol 241:194–220

Ottonello G (1997) Principles of geochemistry. Columbia University Press, New York

Ottonello G, Serva L (eds) (2003) Geochemical baselines of Italy. Pacini, Pisa

Piccarretta G, Zirpoli G (1970) Contributo alla conoscenza delle metamorfiti comprese fra Martirano e Falerna (Calabria). Boll Soc Geol It 89:113–144

Rimstidt JD, Balog A, Webb J (1998) Distribution of trace elements between carbonate minerals and aqueous solutions. Geochim Cosmochim Acta 62:1851–1863

Smedley PL, Kinniburgh DG (2002) A review of the source, behaviour and distribution of arsenic in natural waters. Appl Geochem 17:517–568

Stumm W (1992) Chemistry of the solid–water interface. Wiley, New York

Wagman DD, Evans WH, Parker VB, Schumm RH, Halow I, Bailey SM, Churney KL, Nuttall RL (1982) The NBS tables of chemical thermodynamic properties, selected values for inorganic and C1 and C2 organic substances in SI units. J Phys Chem Ref Data 11(suppl 2):392

White AF, Brantley SL (2003) The effect of time on the weathering of silicate minerals: why do weathering rates differ in the laboratory and field? Chem Geol 202:479–506

Whiting KS (1992) The thermodynamics and geochemistry of arsenic, with application to subsurface waters at the sharon steel superfund site at midvale, Utah. MS Thesis Colorado School of Mines, Golden

Wolery TJ (1979) Calculation of chemical equilibrium between aqueous solutions and minerals: the EQ3/6 software package. Report UCRL-52658, Lawrence Livermore National Laboratory, Livermore

Wolery TJ (1992) EQ3NR, a computer program for geochemical aqueous speciation-solubility calculations: theoretical manual, user's guide and related documentation (version 7.0). Report UCRL-MA-110662 PT III. Lawrence Livermore National Laboratory, Livermore

Wolery TJ, Daveler SA (1992) EQ6, a computer program for reaction path modeling of aqueous geochemical systems: theoretical manual, user's guide, and related documentation (version 7.0). Report UCRL-MA-110662 PT IV. Lawrence Livermore National Laboratory, Livermore